

Preferential Solvent Partitioning within Asphaltenic Aggregates Dissolved in Binary Solvent Mixtures[†]

Vincent J. Verruto and Peter K. Kilpatrick*

Department of Chemical and Biomolecular Engineering, North Carolina State University,
Raleigh, North Carolina 27695

Received September 8, 2006. Revised Manuscript Received December 9, 2006

The heaviest fraction of crude oils, asphaltenes, has been shown to play a central role in the stabilization of troublesome water-in-crude oil emulsions. In previous model oil systems, emulsion stability was observed to depend notably on the properties of self-assembled interfacially active asphaltenic aggregates. Thus, careful characterization of these aggregates is of great importance for better understanding of asphaltene-stabilized emulsions. Small-angle neutron scattering (SANS) has proven to be a powerful tool for such characterization. Described here is the application of SANS on asphaltenes from Hondo crude oil dissolved in binary solvent mixtures of toluene with *n*-heptane, decalin, or 1-methylnaphthalene. A polydisperse oblate cylinder (POC) form factor model was used to fit the aggregate scattering data, and subsequent calculations of minimum error were performed to ascertain the entrained solvent composition within the aggregates. When toluene was paired with either a weak solvent (decalin) or a precipitant (*n*-heptane), the entrained solvent composition was nearly pure toluene (>90%). Conversely, for the toluene/1-methylnaphthalene pairing, methylnaphthalene demonstrated slight preferential entrainment (~60%) compared with the bulk composition (~57%). This is the first such in situ experimental determination of the aggregate composition for asphaltenes dissolved in binary solvents, reinforcing the important role of asphaltene–solvent interactions in asphaltene self-assembly.

Introduction

Asphaltenes comprise a crude oil fraction to which many attribute the stabilization of water-in-crude oil emulsions. The toluene-soluble/*n*-heptane-insoluble fraction of crude oil, asphaltenes, characteristically exhibit fused ring aromaticity with polar heteroatom functionality (pyrroles, phenols, carbonyls, and carboxylic acids).^{1–3} Asphaltenes are inherently heterogeneous and polydisperse in molecular chemistry and size, respectively.^{4,5} Asphaltenes start to self-assemble at modest concentrations (10–50 mg/L),^{6–8} forming interfacially active nanoscale aggregates that diffuse to the oil/water interface and consolidate as an elastic interfacial film that prevents or retards coalescence. Inter-

molecular and intraaggregate interactions are largely due to van der Waals (dispersion) forces and include π – π overlap between aromatic-rich regions of asphaltenes, with possible enhancement of association by Coulombic interactions (H-bonding) among polar oxygenic and nitrogenous moieties.^{1,9} These aggregates, and the emulsions and deposits which result from their properties, have garnered much attention from the petroleum scientific community for their detrimental impact on crude oil transport and processing.

A wide range of experimental investigations have focused on asphaltenic aggregates and their colloidal nature including nanostructure characterization,^{1,10–19} aggregation kinetics,²⁰ adsorption kinetics²¹ and equilibrium,^{22,23} and interfacial

[†] Presented at the 7th International Conference on Petroleum Phase Behavior and Fouling.

* Corresponding author. Office: 919-515-2324. Fax: 919-515-3465. E-mail: peter_kilpatrick@ncsu.edu.

(1) Spiecker, P. M.; Gawrys, K. L.; Kilpatrick, P. K. Aggregation and solubility behavior of asphaltenes and their subfractions. *J. Colloid Interface Sci.* **2003**, *267* (1), 178–193.

(2) McLean, J. D.; Kilpatrick, P. K. Comparison of precipitation and extrography in the fractionation of crude oil residua. *Energy Fuels* **1997**, *11* (3), 570.

(3) Speight, J. G. *The chemistry and technology of petroleum*, 2nd ed.; M. Dekker: New York, 1991; Part xi, p 760.

(4) Yarranton, H. W.; Masliyah, J. H. Molar mass distribution and solubility modeling of asphaltenes. *AIChE J.* **1996**, *42* (12), 3533.

(5) Strausz, O. P.; Peng, P.; Murgich, J. About the colloidal nature of asphaltenes and the MW of covalent monomeric units. *Energy Fuels* **2002**, *16* (4), 809.

(6) Acevedo, S.; Ranaudo, M. A.; Pereira, J. C.; Castillo, J.; Fernandez, A.; Perez, P.; Caetano, M. Thermo-optical studies of asphaltene solutions: evidence for solvent-solute aggregate formation. *Fuel* **1999**, *78* (9), 997–1003.

(7) Goncalves, S.; Castillo, J.; Fernandez, A.; Hung, J. Absorbance and fluorescence spectroscopy on the aggregation behavior of asphaltene-toluene solutions. *Fuel* **2004**, *83* (13), 1823–1828.

(8) Rahmani, N. H. G.; Dabros, T.; Masliyah, J. H. Settling properties of asphaltene aggregates. *Energy Fuels* **2005**, *19* (3), 1099–1108.

(9) Murgich, J. Intermolecular forces in aggregates of asphaltenes and resins. *Pet. Sci. Technol.* **2002**, *20* (9–10), 983–997.

(10) Fenistein, D.; Barre, L.; Broseta, D.; Espinat, D.; Livet, A.; Roux, J. N.; Scarsella, M. Viscosimetric and neutron scattering study of asphaltene aggregates in mixed toluene/heptane solvents. *Langmuir* **1998**, *14* (5), 1013.

(11) Gawrys, K. L.; Kilpatrick, P. K. Asphaltene aggregation: Techniques for analysis. *Instrum. Sci. Technol.* **2004**, *32* (3), 247.

(12) Gawrys, K. L.; Kilpatrick, P. K. Asphaltenic aggregates are polydisperse oblate cylinders. *J. Colloid Interface Sci.* **2005**, *288* (2), 325–334.

(13) Liu, Y. C.; Sheu, E. Y.; Chen, S. H.; Storm, D. A. Fractal Structure of Asphaltenes in Toluene. *Fuel* **1995**, *74* (9), 1352–1356.

(14) Ravey, J. C.; Ducouret, G.; Espinat, D. Asphaltene Macrostructure by Small-Angle Neutron-Scattering. *Fuel* **1988**, *67* (11), 1560–1567.

(15) Roux, J. N.; Broseta, D.; Deme, B. SANS study of asphaltene aggregation: Concentration and solvent quality effects. *Langmuir* **2001**, *17* (16), 5085–5092.

(16) Sheu, E. Y.; Liang, K. S.; Sinha, S. K.; Overfield, R. E. Polydispersity Analysis of Asphaltene Solutions in Toluene. *J. Colloid Interface Sci.* **1992**, *153* (2), 399–410.

(17) Takeshige, W. Hydrodynamic shape and size of Khafji asphaltene in benzene. *J. Colloid Interface Sci.* **2001**, *234* (2), 261–268.

(18) Tanaka, R.; Hunt, J. E.; Winans, R. E.; Thiagarajan, P.; Sato, S.; Takanohashi, T. Aggregates structure analysis of petroleum asphaltenes with small-angle neutron scattering. *Energy Fuels* **2003**, *17* (1), 127.

rheology.^{23–27} An attractive and useful characterization tool for opaque asphaltene solutions is small-angle neutron scattering (SANS), which exploits the neutron scattering contrast between hydrogenated and deuterated materials. In previous SANS investigations of asphaltenic structures in varying solvents, authors have modeled the resulting aggregate morphology as sheets,¹⁴ polydisperse spherical particles,¹⁶ and long rods.²⁸ Several researchers have extracted information about the aggregates without geometric bias using the Guinier analysis, a Lorentzian line shape,²⁹ or a mass fractal form.^{30,31} The Guinier analysis makes no assumptions about an aggregate's geometric shape and is used to obtain the aggregate radius of gyration (R_G), a measure of the mass distribution about the center of mass. The Lorentzian line shape includes only the zero-angle scattering intensity (I_0) and the correlation length (ξ_L) as true fitted parameters.²⁹ In the mass fractal model, an aggregate is described by I_0 , its fractal dimension (d_f), and a characteristic length scale (ξ_{MF}).^{30,31} Recent efforts have explored the form factor models that offer the best fit to different asphaltenic aggregates in different solvent conditions. Tanaka et al. applied spherical, ellipsoidal, and fractal models to Maya, Khafji, and Iranian Light asphaltenes (all *n*-heptane-precipitated) dispersed in decalin, 1-methylnaphthalene, and quinoline at different temperatures.¹⁸ The monodisperse prolate ellipsoid model provided the best cumulative fit of the data in their broad investigation. Gawrys and Kilpatrick performed SANS on *n*-heptane-precipitated Hondo, Canadon Seco, and Arab Heavy asphaltenes in toluene, 40:60 *n*-heptane:toluene, or 90:10 toluene:methanol at room temperature.¹² A comparison of monodisperse and polydisperse spheres, rods, and oblate cylinders identified the polydisperse oblate cylinder (POC) form factor as the best fit for all of the scattering curves. In addition, only the POC model returned values for I_0 and R_G within a mean 10% of the geometry-independent Guinier approximation.

(19) Tanaka, R.; Sato, E.; Hunt, J. E.; Winans, R. E.; Sato, S.; Takanohashi, T. Characterization of asphaltene aggregates using X-ray diffraction and small-angle X-ray scattering. *Energy Fuels* **2004**, *18* (4), 1118–1125.

(20) Hung, J.; Castillo, J.; Reyes, A. Kinetics of asphaltene aggregation in toluene-heptane mixtures studied by confocal microscopy. *Energy Fuels* **2005**, *19* (3), 898–904.

(21) Jeribi, M.; Almir-Assad, B.; Langevin, D.; Henaut, I.; Argillier, J. F. Adsorption kinetics of asphaltenes at liquid interfaces. *J. Colloid Interface Sci.* **2002**, *256* (2), 268.

(22) Ese, M. H.; Yang, X.; Sjoblom, J. Film forming properties of asphaltenes and resins. A comparative Langmuir-Blodgett study of crude oils from North Sea, European continent and Venezuela. *Colloid Polym. Sci.* **1998**, *276* (9), 800.

(23) Yeung, A.; Dabros, T.; Czarniecki, J.; Masliyah, J. On the interfacial properties of micrometre-sized water droplets in crude oil. *Proc. R. Soc. London, Ser. A: Math. Phys. Eng. Sci.* **1999**, *455* (1990), 3709.

(24) Aske, N.; Orr, R.; Sjoblom, J. Dilatational elasticity moduli of water-crude oil interfaces using the oscillating pendant drop. *J. Dispersion Sci. Technol.* **2002**, *23* (6), 809.

(25) Dodd, C. G. The Rheological Properties of Films At Crude Petroleum-Water Interfaces. *J. Phys. Chem.* **1960**, *64* (5), 544.

(26) Freer, E. M.; Radke, C. J. Relaxation of asphaltenes at the toluene/water interface: Diffusion exchange and surface rearrangement. *J. Adhes.* **2004**, *80* (6), 481.

(27) Spiecker, P. M.; Kilpatrick, P. K. Interfacial rheology of petroleum asphaltenes at the oil-water interface. *Langmuir* **2004**, *20* (10), 4022.

(28) Thiagarajan, P.; Hunt, J. E.; Winans, R. E.; Anderson, K. B.; Miller, J. T. Temperature-Dependent Structural-Changes of Asphaltenes in 1-Methylnaphthalene. *Energy Fuels* **1995**, *9* (5), 829.

(29) Mason, T. G.; Lin, M. Y. Asphaltene nanoparticle aggregation in mixtures of incompatible crude oils. *Phys. Rev. E* **2003**, *67* (5), article no. 050401(R).

(30) Hu, X. J.; Littrel, K.; Ji, S.; Pickles, D. G.; Risen, W. M. Characterization of silica-polymer aerogel composites by small-angle neutron scattering and transmission electron microscopy. *J. Non-Cryst. Solids* **2001**, *288* (1–3), 184–190.

(31) Chen, S. H.; Teixeira, J. Structure And Fractal Dimension Of Protein-Detergent Complexes. *Phys. Rev. Lett.* **1986**, *57* (20), 2583–2586.

It should be noted that the many investigations cited above were performed with a wide array of asphaltenes and asphaltene fractions from different crude oils. Asphaltene chemistry (i.e., crude oil source) has been shown to dictate aggregation behavior¹ and interfacial film strength,^{27,32} and it is plausible that different asphaltenes assume different morphologies in solution. However, a definitive molecular description of the aggregate building blocks is absent and a debate continues regarding the fundamental asphaltene molecular architecture. Two popular competing asphaltene molecular models differ in their distribution of the fused aromatic rings and aliphatic moieties. In the “continental” model, asphaltenes are composed of a large polycondensed aromatic center with an aliphatic periphery,^{3,33} whereas the “archipelago” model depicts asphaltenes as smaller polycondensed aromatic “islands” interconnected by aliphatic chains.³⁴ Results from recent studies add to the growing support for the archipelago asphaltene structure. Strausz et al. used gel permeation chromatography to demonstrate the long-time dissociation (days–weeks) of large asphaltene aggregates, presumably due to the large number of intermolecular neighbors (and thus interactions) possible among archipelago-type structures.⁵ A study on asphaltene pyrolysis residues revealed that their saturate, aromatic, and polar aromatic composition was most consistent with the aliphatic-bridged fused aromatic ring model.³⁵ Additionally, recent neutron scattering characterization of asphaltenic aggregates quantified a significant degree of solvent entrainment within aggregates (0.4–0.6 v/v), presumably within cavities and plausible only in archipelago-type asphaltenic aggregates.³⁶

It is important to note that Gawrys and Kilpatrick assumed that the bulk and entrained solvent compositions were equivalent, and for certain solvent mixtures, this is likely to be a reasonable assumption. One might expect, however, that for a nearly equimolar mixture of good and poor solvents, the good solvent will preferentially entrain within the porous aggregate structure over the poor solvent. In such a system, the assumption of equivalent bulk and entrained solvent compositions may be a poor one and thus describe inadequately the precise nature of the aggregate. While others have considered occlusion of hydrocarbons in asphaltenic aggregates using complex fractionation techniques³⁷ or inferring asphaltenic aggregate porosity by settling measurements,⁸ this work is a first regarding this level of asphaltenic aggregate description by an in situ characterization technique like SANS. Here, we describe the use of SANS in the assessment of selective solvent partitioning in asphaltenic aggregates dissolved in binary mixtures of toluene with *n*-heptane, decalin, and 1-methylnaphthalene.

Materials and Methods

Sample Preparation. Asphaltenes were precipitated from Hondo crude oil using an excess of 40 mL of *n*-heptane per gram of crude

(32) McLean, J. D.; Kilpatrick, P. K. Effects of asphaltene aggregation in model heptane-toluene mixtures on stability of water-in-oil emulsions. *J. Colloid Interface Sci.* **1997**, *196* (1), 23.

(33) Groenzin, H.; Mullins, O. C. Molecular size and structure of asphaltenes from various sources. *Energy Fuels* **2000**, *14* (3), 677.

(34) Murgich, J.; Abanero, J. A.; Strausz, O. P. Molecular recognition in aggregates formed by asphaltene and resin molecules from the Athabasca oil sand. *Energy Fuels* **1999**, *13* (2), 278.

(35) Gray, M. R. Consistency of asphaltene chemical structures with pyrolysis and coking behavior. *Energy Fuels* **2003**, *17* (6), 1566.

(36) Gawrys, K. L.; Blankenship, G. A.; Kilpatrick, P. K. Solvent entrainment in and flocculation of asphaltenic aggregates probed by small-angle neutron scattering. *Langmuir* **2006**, *22* (10), 4487–4497.

(37) Liao, Z. W.; Zhou, H. G.; Gracia, A.; Chrostowska, A.; Creux, P.; Geng, A. Adsorption/occlusion characteristics of asphaltenes: Some implication for asphaltene structural features. *Energy Fuels* **2005**, *19* (1), 180–186.

Table 1. Elemental Mass Composition of Asphaltenes (C, H, N, S, and O) Determined by Combustion Analysis^a

sample	%C	%H	%N	%S	%O (by diff)	H/C
HOW	79.10 ± 0.04	8.13 ± 0.02	1.99 ± 0.01	8.22 ± 0.09	2.55 ± 0.05	1.23
HOS-10	79.40 ± 0.14	8.35 ± 0.04	2.03 ± 0.03	7.82 ± 0.23	2.40 ± 0.06	1.25

^a Error values determined from triplicate sample testing. The listed H/C aromaticity is a molar ratio.

Table 2. Hydrogenated/Deuterated Solvent Compositions for Each Solvent Mixture Series^a

toluene			decalin		toluene			<i>n</i> -heptane		toluene			1-MN	
#	ϕ_{hydro}	ϕ_{deut}	ϕ_{hydro}	ϕ_{deut}	#	ϕ_{hydro}	ϕ_{deut}	ϕ_{hydro}	ϕ_{deut}	#	ϕ_{hydro}	ϕ_{deut}	ϕ_{hydro}	ϕ_{deut}
1	0	0.6	0	0.4	1	0	0.6	0	0.4	1	0	0.43	0	0.57
2A	0.03	0.57	0	0.4	2A	0.06	0.54	0	0.4	2A	0.043	0.387	0	0.57
3A	0.06	0.54	0	0.4	3A	0.12	0.48	0	0.4	4A	0.129	0.301	0	0.57
4A	0.09	0.51	0	0.4	4A	0.18	0.42	0	0.4	5A	0.172	0.258	0	0.57
5A	0.12	0.48	0	0.4	5A	0.24	0.36	0	0.4	2B	0	0.43	0.057	0.513
6A	0.15	0.45	0	0.4	2B	0	0.6	0.04	0.36	3B	0	0.43	0.114	0.456
2B	0	0.6	0.02	0.38	3B	0	0.6	0.08	0.32	4B	0	0.43	0.171	0.399
3B	0	0.6	0.04	0.36	4B	0	0.6	0.12	0.28	5B	0	0.43	0.228	0.342
4B	0	0.6	0.06	0.34	5B	0	0.6	0.16	0.24					
5B	0	0.6	0.08	0.32										
6B	0	0.6	0.1	0.3										

^a Note that a "3A" sample was not run for the toluene/methylnaphthalene series. One can easily back out the percentage of a particular solvent that is hydrogenated correspondingly.

and stirred overnight. The precipitated asphaltenes were then filtered using Whatman 542 filter paper and rinsed with *n*-heptane (Fisher, H350-4). An overnight wash of the filtered asphaltenes was performed using boiling heptane in a Soxhlet apparatus until the return to the boiling flask was visually clear. This was immediately followed by an overnight dissolution step using boiling toluene (Fisher, T290-4) in the Soxhlet until the return to the boiling flask was visually clear. The asphaltenes were recovered by evaporation of the toluene in a rotary evaporator (Büchi EL-131) under partial vacuum at 50–60 °C until almost all of the solvent was removed. The asphaltenes were then redissolved with a minimum volume of methylene chloride and transferred to a weighed jar and placed in an exhaust hood. The vapor in the jar was routinely flushed out with argon to minimize oxidation of the asphaltenes. The jar was weighed daily until the mass remained unchanged for consecutive days. These recovered asphaltenes from the whole crude will be referred to as Hondo Whole (HOW) asphaltenes.

In order to obtain a chemical distribution of asphaltenes in which the most polar and insoluble subfraction was present, which would result in a scattering curve with appreciable low-*Q* upturn corresponding to flocculated aggregates,^{1,12} a soluble asphaltene fraction was prepared by precipitating at least 10% of the asphaltenes and using the residual soluble fraction for scattering experiments. From the work of Spiecker et al., this corresponded to a 52.5:47.5 (v:v) mixture of *n*-heptane:toluene for HOW asphaltenes.¹ This was achieved by dissolving 0.67 g of HOW asphaltenes in 35.2 g of toluene and shaking overnight before addition of 30.8 g of *n*-heptane. After additional overnight agitation, the solution was filtered with Whatman 542 filter paper and the filtrate was rotary evaporated, redissolved with minimal methylene chloride, and transferred to a weighed jar to evaporate the solvent. From the recovered asphaltene fraction mass, the actual amount precipitated was 21–23%. This soluble fraction will be referred to as HOS-10 asphaltenes. Both HOW and HOS-10 asphaltenes were sent to the Analytical and Instrumentation Laboratory (Department of Chemistry) at the University of Alberta for elemental analysis on their Carlo Erba EA1108 elemental analyzer. Enough of each sample was sent in order to perform triplicate measurements. The resulting elemental compositions (C, H, N, S, and O) from HOW and HOS-10 are presented in Table 1. It is apparent from the table that the precipitation removes some of the most polar asphaltenes, as the sulfur and oxygen content was lower for HOS-10 than HOW, which is consistent with the recent asphaltene subfractionation work of Gawrys, Blankenship, and Kilpatrick.³⁸

Three sets of asphaltene solutions were prepared in this study: 1 wt % HOW in 40:60 (v:v) decalin:toluene, 1 wt % HOS-10 in 40:60 *n*-heptane:toluene (v:v), and 1 wt % HOW in 50:50 (mol:mol) 1-methylnaphthalene:toluene. The decalin:toluene samples were prepared such that the solvent hydrogenation was adjusted by 5% until a maximum 25% of that particular solvent was hydrogenated, i.e., the first sample was 40:60 *d*-decalin:*d*-toluene and the last was 40:60 *d*-decalin:(75:25 *d*-toluene:*h*-toluene) or 40:60 (75:25 *d*-decalin:*h*-decalin):*d*-toluene. Similarly for the heptane:toluene samples, the hydrogenation of one solvent in successive samples differed by 10% until a maximum 40% of that particular solvent was hydrogenated. In the 1-methylnaphthalene:toluene series, individual solvent hydrogenation differed by 10% among sequential samples up to a maximum of 40% of that individual solvent. To further assist in this description of the samples, the hydrogenated/deuterated solvent mixture compositions for the three mixtures are presented in Table 2. The sum of each row equates to 1, such that the volume fractions presented are out of the total solvent mixture. For samples in the list marked A, toluene was the solvent for which the hydrogenated/deuterated ratio was manipulated, and for samples marked B the second solvent's hydrogenation was controlled. In each series, when comparing the solvent compositions for A and B samples to sample 1, the perdeuterated solvent mixture, the hydrogenated/deuterated composition for a particular solvent in the mixture, requires only a simple calculation and is in accord with the sample preparation description above.

For all mixed solvent systems, the appropriate masses of asphaltenes were first weighed out in small glass jars on an Ohaus Explorer (E12140) laboratory balance. This was followed by the addition of toluene-*d*₈ (CDN Isotopes, 99.7 atom% D) and, when necessary, HPLC grade hydrogenated toluene (Fisher Scientific). Following overnight agitation was the addition of decalin-*d*₁₈ (CDN Isotopes, 98.8 atom% D) and hydrogenated decalin (Acros Organics) to the HOW samples or *n*-heptane-*d*₁₆ (CDN Isotopes, 99.0 atom % D) and HPLC grade hydrogenated *n*-heptane (Fisher Scientific) to the HOS-10 samples. For the 1-methylnaphthalene:toluene samples, either hydrogenated 1-methylnaphthalene (Aldrich) or 1-methylnaphthalene-*d*₁₀ (CDN Isotopes, 98.9 atom% D) was added after initially dissolving HOW in toluene.

Small-Angle Neutron Scattering (SANS). SANS takes advantage of the significantly different neutron scattering cross sections of hydrogenated versus deuterated materials. Isotopic H/D substitution of select materials in an experiment can highlight intra- and interparticle structure, enabling investigations of self-assembled nano- and microstructures in aqueous or organic solvents. The resulting scattering pattern of a sample is related to the Fourier

(38) Gawrys, K. L.; Blankenship, G. A.; Kilpatrick, P. K. On the distribution of chemical properties and aggregation of solubility fractions in asphaltenes. *Energy Fuels* **2006**, *20* (2), 705–714.

transform of the scattering length density distribution. The resulting data in a SANS experiment are typically represented as the scattering intensity, I , as a function of the scattering wavevector, Q , which is the difference between the incident and scattered neutron wavevectors. Here $|Q| = 4\pi\lambda^{-1} \times \sin \theta$, in which λ is the neutron wavelength and 2θ is the scattering angle (this magnitude will be subsequently referred to as Q). The scattering intensity is often expressed simply as the following:

$$I(Q) = N_s P(Q) S(Q) \quad (1)$$

where N_s is the number density of scattering bodies, $P(Q)$ is the scatterer geometric form factor, and $S(Q)$ is the structure factor, a description of the interactions between scatterers. In the dilute-scatterer limit, $S(Q)$ is unity, where modeling efforts are focused on the $P(Q)$ value. For a detailed mathematical description and derivation of the polydisperse oblate cylindrical form factor used in this study the reader should be directed to the work of Gawrys and Kilpatrick.¹²

Samples prepared in mixtures of decalin and toluene were run on the NG3 30m SANS instrument at the Center for High Resolution Neutron Scattering (CHRNS) at the National Institute of Standards and Technology (Gaithersburg, MD). As NIST is a reactor source, the collimated neutron beam is of a single wavelength (i.e., energy) and the accessible Q range can be adjusted by changing the sample-to-detector distance (SDD) and/or the neutron wavelength. For the decalin:toluene samples, the following instrument setup was used: SDD = 230 cm, $\lambda = 6 \text{ \AA}$, $Q_{\min} = 0.0081 \text{ \AA}^{-1}$ ($\sigma Q/Q = 0.286$), $Q_{\max} = 0.2710 \text{ \AA}^{-1}$ ($\sigma Q/Q = 0.062$). Asphaltene solutions dissolved in decalin and toluene were run for 30 min of scattering and corresponding mixed solvent blanks (for background subtraction) were run for 25 min. The 1-methylnaphthalene:toluene samples were run on the NG7 30m instrument with the following setup: SDD = 350 cm, $\lambda = 6 \text{ \AA}$, $Q_{\min} = 0.0091 \text{ \AA}^{-1}$ ($\sigma Q/Q = 0.256$), $Q_{\max} = 0.1806 \text{ \AA}^{-1}$ ($\sigma Q/Q = 0.091$). These solvent mixtures and asphaltene solutions were run on NG7 for 10 min each. Transmissions on all runs at NIST were collected over 2 min.

The heptane:toluene samples were run on the SAND instrument at the Intense Pulsed Neutron Source (IPNS) at Argonne National Lab (Argonne, IL). The IPNS uses a spallation neutron source, in which neutrons of different energies are produced upon the collision of high-energy H^- ions with a depleted uranium target. The SAND is a time-of-flight (TOF) instrument, capable of probing Q values of $0.0035\text{--}0.6 \text{ \AA}^{-1}$. All samples were run in quartz cells having a 2 mm path length. Solutions with heptane and toluene were run for 45 min to 1 h of scattering, and background solvent blanks were run for 45 min. Transmission for each run was collected over 15 min.

Data Reduction and Analysis. The decalin:toluene SANS data were reduced in IGOR Pro (Wavemetrics) using the reduction software package download provided on the NCNR website (http://www.ncnr.nist.gov/programs/sans/data/red_anal.html). The program accounts for transmission of the sample, stray background neutrons in the room, transmission and scattering of the quartz cell, and the detector efficiency to calculate the absolute scattering intensity of the sample. For the heptane:toluene samples, the raw scattering data were reduced with ISAW at the IPNS using a script that subtracted the stray background neutrons and the quartz cell scattering, scaled the data according to the sample transmission, and normalized the data to an absolute intensity scale. Reduced decalin:toluene solvent blank data were fitted with a flat background profile up to $Q = 0.1 \text{ \AA}^{-1}$ to smooth the scattering curve. Because the incoherent cross sections of hydrogenated materials are wavelength-dependent,^{39,40} the background scattering of the partially hydrogenated samples

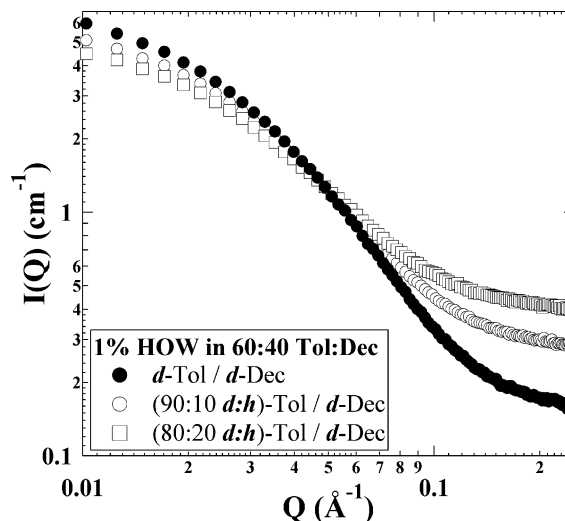


Figure 1. Reduced absolute scattering intensity for a few of the 1 wt % HOW in 40:60 dec:tol series. Note the increasing incoherent background and decreasing low- Q intensity with increasing hydrogenation (decreasing contrast).

from the SAND instrument did not have a flat background profile, so the curves were fit with an arbitrary equation over the Q range $0.01\text{--}0.5 \text{ \AA}^{-1}$, only for the purposes of smoothing the data.

To conserve valuable beam time, we only prepared mixed solvent backgrounds at every 10% hydrogenation of each solvent with the intent of interpolating the intermediate background samples for the decalin:toluene series. This was easily achieved with the flat data of the decalin:toluene solvent samples in the relevant Q range. Plotting the incoherent intensity (I_{inc}) as a function of the h -decalin or h -toluene mole fraction, we then fit this data with an arbitrary function for interpolative use. Using the mole fraction of the hydrogenated solvent from the solution sample preparation, the appropriate I_{inc} could then be calculated from the fit for the intermediate solvent blanks that were not subjected to scattering. For the smoothed $I_{\text{inc}}(Q)$ for the heptane:toluene solvent mixture backgrounds, entire curves were used to interpolate the background contribution of intermediate solvent mixtures.

Smoothed mixed solvent scattering data were subsequently subtracted from the corresponding reduced asphaltene solution scattering curves. These subtracted data were then subject to a fitting routine using the POC model in Igor Pro described by Gawrys and Kilpatrick,¹² with the splice point at $Q \times R_{\text{cyl}} = 2.1$. We should note, as a reminder, that SANS data from polydisperse systems like asphaltenes have been fitted with a variety of approximations and geometry-specific descriptions. Our past experience using the POC model has, in our opinion, enabled a more detailed description of asphaltenic aggregates (e.g., shape and solvent entrapment) and is the basis for much of the interpretation regarding the scattering data reported in the next section.

Results and Discussion

1% HOW in 40:60 (v:v) Decalin:Toluene. A small set of scattering curves for 1% HOW in 40:60 decalin:toluene are shown in Figure 1, for which we see the effects of partially hydrogenating the solvent mixture. As expected, we observed an increase in the incoherent background (high Q) as the hydrogen content was increased, as well as a reduction in the low- Q intensity (I_0) as a result of the reduced aggregate/solvent contrast. Model representations of the background subtraction and the subsequent optimized POC curve are presented in Figure 2. Expecting that chemically identical HOW solutions—only the degree of hydrogenation of the solvent differed—would have identical aggregate dimensions, we simultaneously fit all of the curves with the constraint that R_{cyl} , σ_R , and L_{cyl} were the same

(39) May, R. P.; Ibel, K.; Haas, J. The Forward Scattering of Cold Neutrons by Mixtures of Light and Heavy-Water. *J. Appl. Crystallogr.* **1982**, *15* (Feb), 15–19.

(40) Knoll, W.; Schmidt, G.; Ibel, K. Incoherent-Scattering Corrections for Forward Scattering of Neutrons by Aqueous Buffers - Temperature-Dependence and Influence of Absorbing Salts. *J. Appl. Crystallogr.* **1985**, *18* (Apr), 61–64.

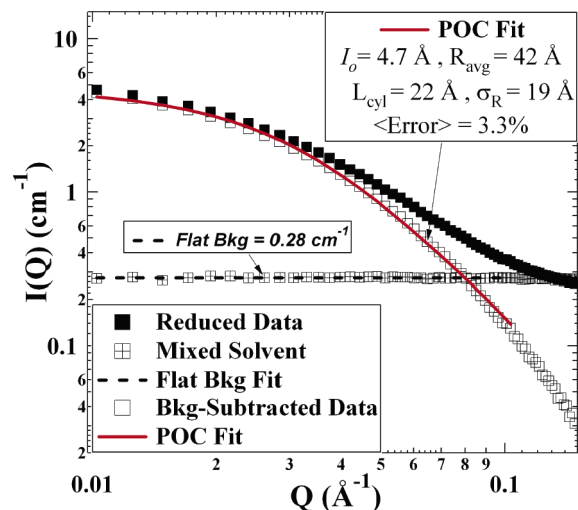


Figure 2. Typical background subtraction for 1 wt % HOW in 40:60 dec:tol samples. Asphaltene data were reduced in IGOR Pro and are represented as absolute scattering intensity (solid box) versus Q . Mixed solvent blanks (box with plus sign) were fit with to a flat profile (dotted black line). Subtraction of the flat bkg from the reduced data yielded a background-free scattering curve (open box), for which a POC fit (solid red line) was applied.

for all samples. The resulting fitted parameters minimized the average percent error over all of the data points used in the fit, i.e.

$$\langle \% \text{ Error} \rangle = \frac{\sum_n \left| \frac{I_{\text{data}} - I_{\text{POC}}}{I_{\text{data}}} \right|_i}{n} \times 100 \quad (2)$$

where I_{data} is the reduced absolute scattering intensity, I_{POC} is the scattering intensity predicted by the model, and n is the total number of points for all of the fits (in this case 11 curves \times 42 points = 462). The Guinier I_0 for each sample was used as the POC I_0 , and the background was fixed at zero for all of the data sets in the series. The resulting optimized fit returned $R_{\text{cyl}} = 42.1 \text{ \AA}$, $\sigma_R = 19.2 \text{ \AA}$, and $L_{\text{cyl}} = 22.4 \text{ \AA}$, having a minimized average error of 4.4%.

In order to assess the entrained solvent composition, we initially sought to solve for the total entrainment as a function of the toluene volume fraction in the entrained solvent. This was achieved by solving the objective function shown below.

$$\frac{M_w(I_{0,\text{fit}}) - M_w(I_{0,\text{calc}})}{M_w(I_{0,\text{fit}})} \leq 10^{-7} \quad (3)$$

$M_w(I_{0,\text{fit}})$ and $M_w(I_{0,\text{calc}})$ are the apparent aggregate molecular weights determined by the fitted POC I_0 value and the calculated I_0 using the POC parameters, respectively, defined by¹²

$$M_w(I_0) = \frac{I_0 N_A \rho_{m,\text{agg}}}{\phi_{\text{agg}} (\Delta\rho)^2} \quad (4)$$

$$I_{0,\text{calc}} = \phi_{\text{agg}} (\Delta\rho)^2 \pi R_{\text{cyl}}^2 L_{\text{cyl}} \frac{(z+4)(z+3)}{(z+1)^2} \quad (5)$$

where ϕ_{agg} is the aggregate volume fraction, N_A is Avogadro's number, $\rho_{m,\text{agg}}$ is the mass density of the aggregate, $(\Delta\rho)^2$ is the squared difference of the aggregate and solvent scattering length densities, R_{cyl} is the average cylinder radius, L_{cyl} is the

cylinder length, and z is the radial polydispersity index defined as $z = (R_{\text{cyl}}/\sigma_R)^2 - 1$. Note that the total amount of entrained solvent and its composition should affect $\rho_{m,\text{agg}}$, $(\Delta\rho)^2$, and ϕ_{agg} .

Thus for each sample, we constructed a curve representing the total entrained solvent as a function of entrained solvent composition. For ideal, monodisperse aggregates of identical chemical composition in which the entrained solvent is well-mixed and uniformly distributed, one should expect these curves to all intersect at one unique point, defined by the total solvent entrainment and the entrained solvent composition. However, no single locus was observed for the intersection of all of the curves.

Ever mindful of nonidealities inherent in asphaltenic systems, polydispersity and chemical heterogeneity, we tabulated the average percent error over all sample curves for each of 3321 unique combinations of total entrainment ($\Phi_{\text{entrainment,total}} = 0\text{--}80\%$, 1% steps) and entrained solvent composition ($\phi_{\text{toluene,ent}} = 0\text{--}1$, 0.025 steps). For every element in this 81×41 matrix of total percent entrained solvent and entrained solvent compositions, we calculated the new $I_{0,\text{calc}}$ for each sample using the optimized R_{cyl} , L_{cyl} , and σ_R parameters as well as $\rho_{m,\text{agg}}$, $(\Delta\rho)^2$, and ϕ_{agg} now adjusted for the new values of $\Phi_{\text{entrainment,total}}$ and $\phi_{\text{toluene,ent}}$. Then using all of these parameters, we calculated a POC curve for each sample and assigned an average error from eq 2 for each combination of $\Phi_{\text{entrainment,total}}$ and $\phi_{\text{toluene,ent}}$. From this array of average errors, we located the global minimum, which defined a region of total entrainment and entrained solvent composition that characterize the HOW asphaltenic aggregates. In the contour plot shown in Figure 3A, this narrow region is defined by the filled oval that spans $\phi_{\text{toluene,ent}} = 0.85\text{--}1$ and $\Phi_{\text{entrainment,total}} = 12\text{--}14\%$. Inspecting the average error as a function of total entrained solvent at an entrained solvent composition of 95% toluene reveals the minimum error occurs at 13% total entrained solvent, as shown in Figure 3B. Figure 3C exhibits the error as a function of the entrained solvent composition at $\Phi_{\text{entrainment,total}} = 13\%$, for which the minimum error occurs at $\phi_{\text{toluene,ent}} = 0.95$.

1% HOS-10 in 40:60 (v:v) *n*-Heptane:Toluene. A similar optimization was performed on the HOS-10 samples in 40:60 heptane:toluene, for which all background subtracted data were simultaneously fit to share R_{cyl} , σ_R , and L_{cyl} while allowing I_0 and the background to vary independently. The resulting optimized parameters yielded $R_{\text{cyl}} = 51.0 \text{ \AA}$, $\sigma_R = 23.6 \text{ \AA}$, and $L_{\text{cyl}} = 25.9 \text{ \AA}$, with an average error of 6.1%. Having been dispersed in a poorer solvent mixture, even though they were of a more soluble subfraction, the aggregates were $\sim 70\%$ larger than those for the HOW in 40:60 decalin:toluene samples, with comparable polydispersity. As was observed in the decalin:toluene series, there was no single intersection point for all of the samples regarding the total entrainment as a function of the entrained solvent composition. However, Figure 4A–C illustrates that the minimum average error indicates a total solvent entrainment of 37% ($V_{\text{ent}}/V_{\text{agg}}$) that appears to be nearly pure toluene (95–100%).

1% HOW in 50:50 (mol:mol) 1-Methylnaphthalene:Toluene. Data for the equimolar 1-methylnaphthalene/toluene mixture series were subjected to the same aforementioned optimization routine. Here, background-subtracted data were simultaneously fit to share R_{cyl} , σ_R , and L_{cyl} while allowing I_0 to vary and bkg to remain zero. The optimization yielded $R_{\text{cyl}} = 38.5 \text{ \AA}$, $\sigma_R = 17.6 \text{ \AA}$, and $L_{\text{cyl}} = 22.4 \text{ \AA}$, with an average error of 8.8%. Of the three solvent mixtures, asphaltenic aggregates in this series had the smallest geometric dimensions and overall $\langle R_G \rangle$. Presented in Figure 5A is the calculated

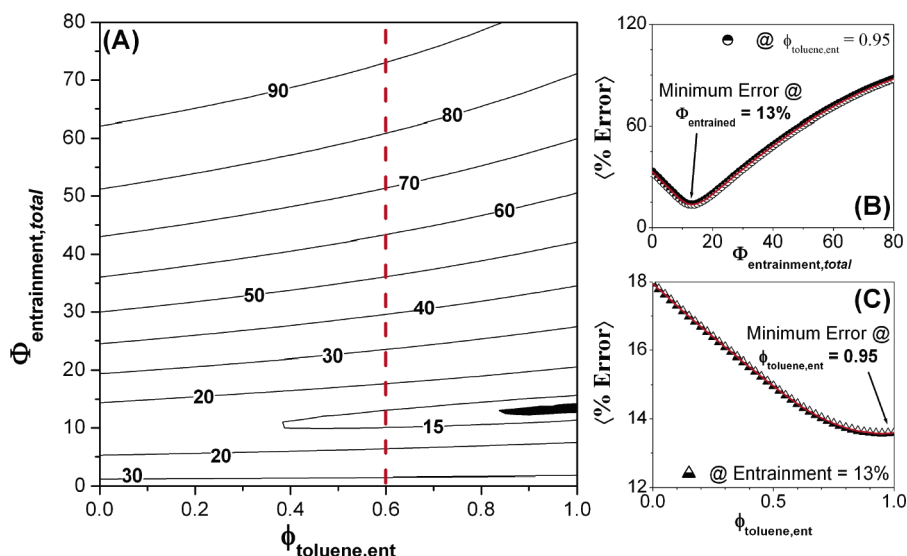


Figure 3. (A) Contour plot of $\langle\% \text{ Error}\rangle$ (eq 2) as a function of total entrainment and entrained solvent composition for the 1% HOW in 40:60 decalin:toluene series. (B) Average error as a function of total entrainment at $\phi_{\text{toluene, ent}} = 0.95$. (C) Average error as a function of entrained solvent composition at $\Phi_{\text{entrainment}} = 13\%$.

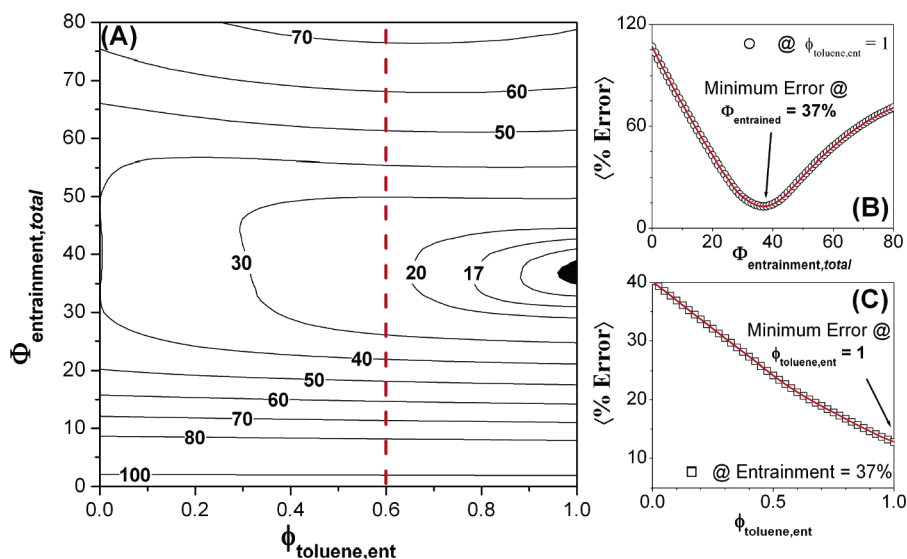


Figure 4. (A) Contour plot of $\langle\% \text{ Error}\rangle$ (eq 2) as a function of total entrainment and entrained solvent composition for the 1% HOS-10 in 40:60 heptane:toluene solvent mixtures. The vertical dashed line represents the average bulk solvent composition. (B) Average error as a function of total entrainment at $\phi_{\text{toluene, ent}} = 1$. (C) Average error as a function of entrained solvent composition at $\Phi_{\text{entrainment}} = 37\%$.

minimum error contour plot for 1% HOW asphaltenes in the equimolar mixture of 1-methylnaphthalene and toluene, along with the average bulk solvent composition (red dashed line). It is apparent from the plots in Figure 5A–C that the methylnaphthalene composition in the entrained solvent is marginally greater than that of the bulk, 60 to 57% (v/v), respectively.

Rationale for Observed Selective Partitioning. In each of the three asphaltenic aggregate systems presented above, the bulk solvent contained a mixture of toluene and a cosolvent of varying quality (cf. Table 3). Calculations of the POC aggregate average radius of gyration were performed using¹²

$$\langle R_G \rangle^2 = \frac{L_{\text{cyl}}^2}{3} + \frac{R_{\text{cyl}}^2}{2} \frac{(z+6)(z+5)}{(z+1)^2} \quad (6)$$

These cosolvents differ in several ways including their solubility parameters, density, and molecular size and shape. Of these solvents, 1-methylnaphthalene is considered to be the best solvent for asphaltenes, which is consistent with the observation

that HOW aggregates have the smallest $\langle R_G \rangle$ and $\langle V_{\text{agg}} \rangle$ in this solvent. By this criterion, solvent quality or asphaltene solvency decreases in the sequence methylnaphthalene, toluene, decalin, and *n*-heptane, which, by definition, is an asphaltene antisolvent (precipitant). Considering the solvent H/C molar ratio, which we use as an “aromaticity index”, we observe that with decreasing H/C the solvents used here become increasingly aromatic, as well as increasingly better solvents for asphaltenes. Presented in Table 4, in which the solvents are listed from left-to-right with respect to increasing asphaltene solvency, are some of these defining attributes of the solvents used in this study.

One should expect the asphaltene–solvent and asphaltene–asphaltene intermolecular interactions to dictate the observed equilibrium aggregate structures in these SANS experiments. From Tables 3 and 4, we see that HOW aggregates in toluene have an $\langle R_G \rangle$ of roughly 51 Å, with aggregates of the HOS-10 fraction expected to be slightly smaller. At the compositions studied, adding a solvent like *n*-heptane or decalin results in individual aggregates with an increased average volume (1.3–

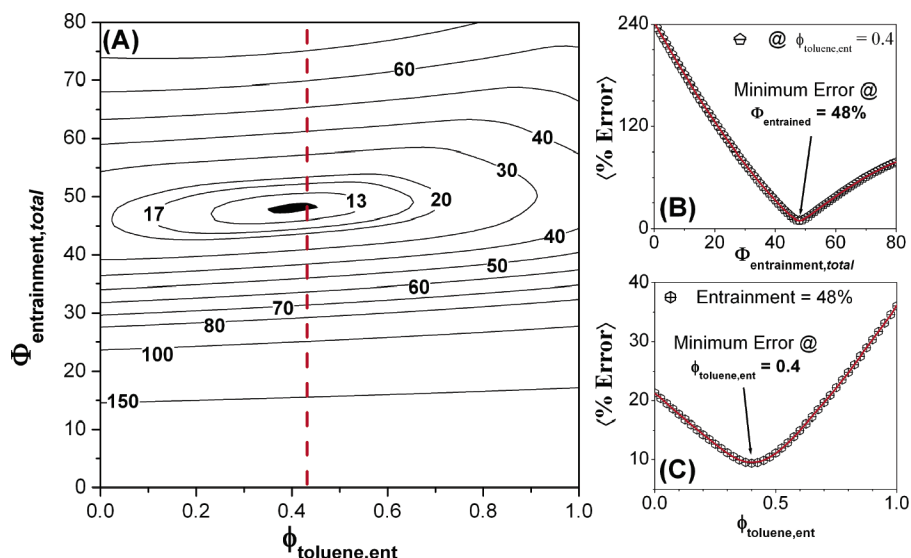


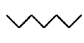
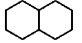
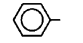
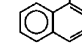
Figure 5. (A) Contour plot of (% Error) (eq 2) as a function of total entrainment and entrained solvent composition for the 1 wt % HOW in 43:57 (v:v) 1-methylnaphthalene:toluene samples. The vertical dashed line represents the average bulk solvent composition. (B) Average error as a function of total entrainment at $\phi_{\text{toluene, ent}} = 0.4$. (C) Average error as a function of entrained solvent composition at $\Phi_{\text{entrainment}} = 48\%$.

Table 3. POC Aggregate Dimensions for 1 wt % HOW or HOS-10 Asphaltene Solutions Described in this Study^a

solvent	R_{cyl}	σ_{R}	L_{cyl}	$\langle R_{\text{G}} \rangle$	$\langle \text{Error} \rangle$	$\Phi_{\text{ent, total}}$	$\phi_{\text{toluene, ent}}$
toluene- d_8	40.6	18.3	20.5	56.1		36%	1
decalin- d_{18}	52.0	23.5	26.1	72.1		27%	N/A
1-methylnaphthalene- d_{11}	34.5	15.3	14.6	46.7		40%	N/A
40:60 decalin:toluene	42.1	19.2	22.4	59.0	4.4%	13%	0.85–1
40:60 heptane:toluene ^b	51.0	23.6	25.9	72.3	6.1%	37%	0.95–1
43:57 methylnaphthalene:toluene	38.5	17.6	22.4	54.3	8.8%	48%	0.4

^a All POC dimensions are in units of angstroms (Å). $\langle R_{\text{G}} \rangle$ was calculated using eq 6. The listed solvent ratios are volumetric. ^b HOS-10 asphaltene solution.

Table 4. Distinctive Properties of the Four Organic Solvents Used in this Study^a

	<i>n</i> -heptane	decalin	toluene	1-MN
molecular structure				
ρ_{mass}^b (g/cm ³)	0.68 [0.79]	0.90 [1.01]	0.86 [0.93]	1.00 [1.12]
$\delta_{\text{D}}, \delta_{\text{P}}, \delta_{\text{H}}$ (J ^{0.5} /cm ^{1.5}) ^c	15.3, 0, 0	18.4, 0, 0	18, 1.4, 2	20.6, 0.8, 4.7
H/C (mol/mol)	2.29	1.80	1.14	0.91
$\langle V_{\text{agg}} \rangle$ (nm ³)		267	128	65
$\langle R_{\text{G}} \rangle$ (Å)		72	56	47
ρ_{neutron} (x10 ⁻⁶ Å ⁻²)	-0.544 [6.29]	-0.00329 [7.27]	0.934 [5.61]	1.51 [6.04]

^a Bracketed values are for perdeuterated species. The solvents are presented from left to right with respect to increasing asphaltene solubility.

^b At 25 °C from ref 43. ^c Reference 44.

2.1×) and average surface area (1.7–2.5×). On the basis of a mass balance, this would decrease the total number of aggregates as well as the total aggregate surface area in contact with the solvent. It is understood that aggregate size grows with the addition of *n*-heptane until the aggregates flocculate and subsequently precipitate when they become too large to remain suspended by the thermal energy of the system.¹ This response by the asphaltenes is driven by the minimization of the free energy resulting from solvent–aggregate interactions. It is possible that the aliphatic portions of the asphaltenes present at the aggregate surface rearrange and extend into the bulk to further reduce the solvent–aggregate interaction free energy.

Since asphaltenes are prepared by heptane-induced precipitation from a crude oil, the interaction between the polynuclear aromatic moieties on the asphaltene and *n*-heptane must be thermodynamically unfavorable. Rearrangement of the flexible aliphatic chains could minimize association with the condensed aromatic groups in the aggregate, effectively shielding the inner aggregate from *n*-heptane exposure.

When decalin was paired with toluene, we observed only a slight amount of decalin entrained within the aggregates. While decalin is aliphatic in nature, its cyclic structure renders it a solvent for asphaltenes, albeit a weak one. Table 3 shows a comparison of the $\langle R_{\text{G}} \rangle$ calculated using the POC parameters for HOW asphaltenes in the different pure solvents listed. In decalin alone, HOW aggregates are considerably larger than those in toluene or 1-methylnaphthalene. Unlike *n*-heptane, however, decalin does not induce asphaltene precipitation upon addition. This suggests that the interactions between decalin and the polynuclear moieties in the asphaltenic aggregate are more favorable than the same interactions between these moieties and *n*-heptane. This is likely a result of the presence of fused naphthenic and alicyclic rings observed in asphaltenes.⁵ We see in Table 4 that for decalin the Hansen solubility parameter related to dispersion has a value nearly equivalent to toluene yet substantially larger than that of *n*-heptane. However, polar or H-bonding contributions to the solubility parameters, which are present in toluene and 1-methylnaphthalene, are absent in decalin and hence limit its asphaltene solvency. It should be noted that although it is drawn flat in Table 4, decalin actually exists in *cis* and *trans* forms, neither of which are planar molecules like methylnaphthalene or toluene, and each occupy molecular volume differently. Additionally, lacking delocalized

π orbital electrons ubiquitous in aromatic species, decalin does not associate with fused aromatic moieties as favorably as toluene or methylnaphthalene. This is consistent with solubility data for naphthalene, the simplest fused aromatic ring molecule, in benzene⁴¹ (38 mol %) versus *cis*-decalin⁴² (27 mol %) at $\sim 35^\circ\text{C}$, as well as a comparison of the universal quasichemical (UNIQUAC) activity coefficient model binary interaction parameters for naphthalene in *cis*-decalin versus tetralin.⁴² As a result, entrained decalin within an aggregate is unlikely to reside stacked between condensed aromatic regions of asphaltene when toluene is also present.

Also of interest is that the total solvent entrainment for the HOW aggregates in the decalin:toluene mixture is appreciably lower than HOW in pure toluene or HOS-10 in 40:60 heptane:toluene. Observe in Table 3 that the average aggregate volume for the decalin:toluene samples is about the same for HOW in toluene but is significantly less than HOS-10 in 40:60 heptane:toluene. It seems that two competing factors are at play here: (1) the tendency for total solvent entrainment to increase with increasing aggregate size and (2) the less favorable thermodynamic interactions of decalin with polynuclear aromatic moieties. This is evident in Table 3 when we compare the total entrainment values for HOW and HOS-10 in single and mixed solvents. For HOW in strong solvents like toluene and methylnaphthalene, the favorable aromatic stacking interactions lead to $\sim 40\%$ entrainment. When dissolved in a mixture of heptane and toluene, the aggregates are much larger, which should mean more entrainment pockets and higher total entrainment. However, the unfavorable asphaltene interactions with heptane limit this entrainment to roughly that of pure toluene. For the decalin:toluene solvent mixture, the aggregate size increases slightly, but the less favorable association with between asphaltene and decalin leads to a lower total entrainment. The key question is the following: why does the entrainment differ so greatly among the mixtures studied? This must be related to the specific asphaltene-solvent interactions and, to some degree, solvent-solvent interactions. Since asphaltene is soluble in decalin, decalin-asphaltene interactions must be favorable relative to heptane-asphaltene interactions, although much less favorable than those between toluene or methylnaphthalene and asphaltene. Thus, decalin entrains to a higher degree than heptane—5–15% compared to 0–5% for heptane—and the less favorable thermodynamics drive the total entrainment to about $1/3$ of that of pure toluene. This argument applies for HOW in pure decalin in which the average aggregate volume is almost double that for pure toluene, while the total entrainment is $3/4$ of the value obtained for pure toluene. This effect may be amplified in this mixture as the decalin likely interferes with the toluene-asphaltene and toluene-toluene stacking interactions, negatively impacting the total entrainment.

Intuitively, when two aromatic solvents were paired together in equimolar contribution, toluene and 1-methylnaphthalene, the contour plot in Figure 5A describes only a slight enhancement of the methylnaphthalene composition within the aggregates. Again, from Tables 3 and 4, we have inferred that 1-methylnaphthalene is the strongest solvent of those tested, i.e., it induces aggregates of the smallest dimensions. This should be

expected using a “like dissolves like” interpretation coupled with inspection of the dispersion, polar, and H-bonding Hansen solubility parameters (Table 4) in comparison to those for toluene. Although noticeable, the enhanced solvency of asphaltene in methylnaphthalene versus toluene is small, and as a result, the extent to which it is preferentially entrained also is small. This is an encouraging result, as the ordering of preferential entrainment seems to agree with the ordering of solvents in Table 4. This means that the preferential entrainment of toluene decreases as toluene is paired with solvents of increasing asphaltene solvency, solvents listed from left-to-right in Table 4, and when paired with an even better solvent, the better solvent is preferentially entrained.

Perhaps a more general observation is that in a pairing of any two solvents, the one having the most favorable thermodynamic association with asphaltene appears to be preferentially entrained within the aggregate. However, one might expect the entrained composition to be a function of the bulk composition, such that the degree to which one solvent preferentially entrains is different for varying ratios of a bulk solvent mixture. Overall, the results suggest that by considering a few simple, yet important, properties of individual solvents, we can better understand, and perhaps predict, how they impact the aggregation state of asphaltene dissolved in binary or higher order solvent mixtures.

Conclusions

Through the application of SANS on asphaltene solutions, we can probe aggregate structure with great detail. In this work we have demonstrated that, for asphaltene aggregates in binary solvent mixtures of a good and poor solvent, the assumption of equivalent composition for the bulk and entrained solvent is invalid. In fact, we observed the preferential enhancement of the toluene entrainment within aggregates in both the decalin:toluene and *n*-heptane:toluene solvent pairings, i.e., the toluene composition of the entrained solvent exceeded that of the bulk solvent. Alternatively, for a binary mixture of chemically similar strong solvents, toluene and 1-methylnaphthalene, the experimental observation was a slight preferential enhancement of 1-methylnaphthalene entrained composition within the aggregates. Though intuitive in nature, these results highlight the importance of the asphaltene-solvent interactions that clearly influence the aggregation state, when dissolved in not only a single solvent but also binary mixtures of solvents of varying quality. To our best knowledge, this is the first time such in situ experimental observations regarding preferential solvent entrainment within asphaltene has been documented in the literature.

Acknowledgment. This research was supported by the Petroleum Environmental Research Forum, ExxonMobil, Shell, Equilon, Chevron-Texaco, Nalco Energy Services Division, Champion Technologies, and National Science Foundation Grants (TSE-0124760). This work benefited from the use of facilities supported in part by the National Science Foundation under Agreement No. DMR-9986442. We acknowledge the support of the National Institute of Standards and Technology, U.S. Department of Commerce, in providing the neutron research facilities used in this work. In particular, we would like to thank Boualem Hammouda and Min Lin. This work benefited from the use of facilities in the Intense Pulsed Neutron Source and the Chemistry Division, which is funded by the U.S. Department of Energy, Office of Basic Energy Sciences, under contract W-31-109-ENG-38 to the University of Chicago. We would particularly like to thank Pappannan Thiagarajan and Denis Wozniak of the Intense Pulsed Neutron Source Division at Argonne National Laboratory for their assistance with the SAND

(41) McLaughlin, E.; Zainal, H. A. The Solubility Behaviour of Aromatic Hydrocarbons in Benzene. *J. Chem. Soc.* **1959**, (Mar), 863–867.

(42) Gupta, A.; Gupta, S.; Groves, F. R.; McLaughlin, E. Correlation of Solid Liquid and Vapor-Liquid-Equilibrium Data for Polynuclear Aromatic Compounds. *Fluid Phase Equilib.* **1991**, *64*, 201–211.

(43) Smallwood, I. M. *Handbook of Organic Solvents*; Wiley & Sons: New York, 1996.

(44) Hansen, C. M. *Hansen Solubility Parameters: A User's Handbook*; CRC Press: Boca Raton, FL, 2000.

instrument. We would also like to thank Wayne Moffat of the University of Alberta, Department of Chemistry, for elemental analysis of the asphaltenes. Additionally, we wish to thank Keith Gawrys for helpful discussions regarding his POC model and fitting with the IGOR program. For their help in sample prep and

instrument operation, we would like to acknowledge Matthew Smith and Salomon Turgman.

EF060456N